# Stem Cell Reports Article



**-OPEN ACCESS** 

## JAK/STAT signaling promotes the emergence of unique cell states in ulcerative colitis

Grzegorz Maciag,<sup>1,7</sup> Stine Lind Hansen,<sup>1,7</sup> Kata Krizic,<sup>1,7</sup> Lauge Kellermann,<sup>2</sup> Maureen Joy Inventor Zøylner,<sup>1</sup> Svetlana Ulyanchenko,<sup>1</sup> Martti Maimets,<sup>1</sup> Astrid Møller Baattrup,<sup>1</sup> Lene Buhl Riis,<sup>3</sup> Konstantin Khodosevich,<sup>4</sup> Toshiro Sato,<sup>5,6</sup> Raul Bardini Bressan,<sup>1,\*</sup> Ole Haagen Nielsen,<sup>2,\*</sup> and Kim B. Jensen<sup>1,4,8,\*</sup>

#### **SUMMARY**

The intestinal epithelium ensures uptake of vital nutrients and acts as a barrier between luminal contents and the underlying immune system. In inflammatory bowel diseases, such as ulcerative colitis (UC), this barrier is compromised, and patients experience debilitating symptoms. Here, we perform single-cell RNA profiling of epithelial cells and outline patterns of cell fate decisions in healthy individuals and UC patients. We demonstrate that patterns of hierarchical behavior are altered in UC patients and identify unique cellular states associated with Janus kinase/signal transducer and activator of transcription (JAK/STAT) activation in ulcerated and non-ulcerated areas of the colonic epithelium. These transcriptional changes could be recapitulated in human colonic organoids, wherein cytokine-mediated activation of JAK/STAT led to the emergence of cell populations with augmented regenerative properties. Altogether, our findings indicate that intricate relationships between epithelial and cytokine signaling regulate cell fate during epithelial tissue regeneration in humans and have important implications for the understanding of UC biology.

#### **INTRODUCTION**

The epithelial lining of the colon forms the physical barrier protecting our body against the microbes and food antigens present within the lumen (Gehart and Clevers, 2019). The epithelium is maintained by intestinal stem cells (ISCs) that reside at the bottom of crypts giving rise to proliferating progenitors, which differentiate into absorptive colonocytes and secretory cells, including mucus-producing goblet cells and hormone-secreting enteroendocrine cells (EECs) (de Sousa and de Sauvage, 2019). Upon damage the epithelial barrier heals rapidly to restore its protective function. Any delay in healing can promote sustained inflammation, which triggers further damage and increases the risk of developing inflammatory bowel disease (IBD), including ulcerative colitis (UC) (Le Berre et al., 2023). Although our understanding of disease etiology and factors influencing UC development and progression is gradually increasing (Graham and Xavier, 2020), it remains unclear how cell fate is regulated at sites of injury.

Advances in single-cell profiling approaches have provided novel insights into the cellular complexity of the colonic tissue. This includes detailed analysis of colonic

mesenchyme during homeostasis and ulceration (Kinchen et al., 2018), identification of a new subtype of epithelial cells in the homeostatic epithelium (Parikh et al., 2019), and mapping potential interactions between epithelial, immune, and stromal cells (Smillie et al., 2019). However, the principles governing maintenance of the human colonic epithelium, and how this is affected in UC, are incompletely understood. Most of our knowledge about cellular behavior originates from studies using murine models. These studies support a hierarchical model, where ISCs during homeostasis fuel tissue replenishment (Beumer and Clevers, 2021), whereas upon damage cells deviate significantly from these patterns of cell behavior with evidence of cellular dedifferentiation (Yui et al., 2018). Although, analyses have mapped expression of fetal-like gene signature in IBD tissue (Elmentaite et al., 2020; Fawkner-Corbett et al., 2021), the cell fate changes associated with ulceration in patients are largely unexplored.

Mechanistically, numerous signaling pathways linked with cell-state changes have been implicated in tissue regeneration (Larsen and Jensen, 2021). How the human colonic epithelium responds to damage, however, remains to be resolved at both the cellular and molecular level. To address these questions, we analyzed the epithelium of



<sup>&</sup>lt;sup>1</sup>Novo Nordisk Foundation Center for Stem Cell Medicine (reNEW), Faculty of Health and Medical Sciences, University of Copenhagen, 2200 Copenhagen N, Denmark

<sup>&</sup>lt;sup>2</sup>Department of Gastroenterology, Herlev Hospital, University of Copenhagen, 2730 Herlev, Denmark

<sup>&</sup>lt;sup>3</sup>Department of Pathology, Herlev Hospital, University of Copenhagen, 2730 Herlev, Denmark

<sup>&</sup>lt;sup>4</sup>Biotech Research and Innovation Centre, University of Copenhagen, 2200 Copenhagen N, Denmark

<sup>&</sup>lt;sup>5</sup>Department of Organoid Medicine, Keio University School of Medicine, Tokyo, Japan

<sup>&</sup>lt;sup>6</sup>Department of Gastroenterology, Keio University School of Medicine, Tokyo, Japan

<sup>&</sup>lt;sup>7</sup>These authors contributed equally

<sup>&</sup>lt;sup>8</sup>Lead contact

<sup>\*</sup>Correspondence: raul.bressan@sund.ku.dk (R.B.B.), ohn@dadlnet.dk (O.H.N.), kim.jensen@sund.ku.dk (K.B.J.) https://doi.org/10.1016/j.stemcr.2024.06.006



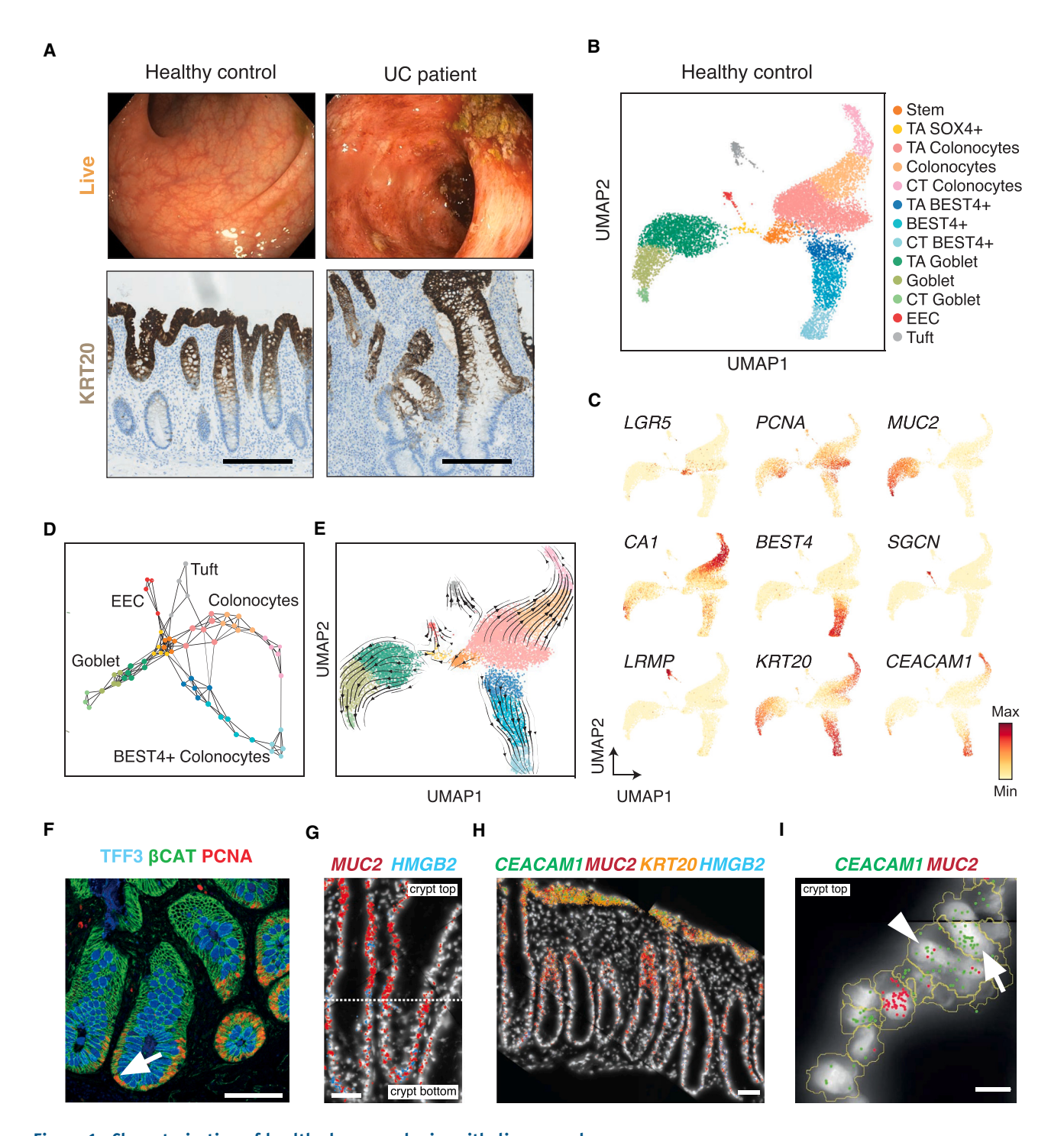


Figure 1. Characterization of healthy human colonic epithelium samples

- (A) Representative images of live colonoscopy (top) and histological analysis (bottom) confirming ulceration in the epithelium of UC patients (bottom). Histological samples were stained for the gastrointestinal epithelium marker KRT20 and counterstained with hematoxylin. Scale bar:  $100 \mu m$ .
- (B) UMAP plot of 11,035 colonic epithelial cells profiled from healthy samples following annotation based on expression of cell lineage markers.
- (C) UMAP plots highlighting expression of known lineage markers in the cell type clusters identified in (B).



healthy individuals and patients with UC using single-cell RNA sequencing (scRNA-seq) and utilized human colonic organoids to model predictions made from the computational analyses. We show that distinct progenitors are the main driving source of tissue renewal during homeostasis and that normal patterns of cell fate decisions are disrupted in UC. Furthermore, we identify unique inflammationassociated (IA) cell states in the epithelium of patients with UC, which are linked with Janus kinase/signal transducer and activator of transcription (JAK/STAT) activation. Using human colonic organoids, we provide evidence that cytokine-induced JAK/STAT activation leads to emergence of IA states and increases regenerative features in vitro. Conversely, pharmacological inhibition of JAK impairs functional recovery in a mouse colitis model in vivo. Collectively, our study suggests that unique cellular states play a role in the regeneration of the colonic epithelium in ulcerative conditions.

#### **RESULTS**

### Profiling of human colonic epithelial cells in healthy individuals

To outline the cellular composition and patterns of cell fate decisions in the healthy and diseased colonic epithelium, we profiled biopsies of the sigmoid colon from healthy individuals (n = 4) and patients with UC in active disease stage (n = 4) by scRNA-seq (Figures 1A and S1A–S1C). We first focused on the dataset generated from the healthy individuals (11,035 epithelial cells) to establish the baseline under a homeostatic condition (S1A-C; Table S1). Cluster analysis combined with expression of cell type-specific markers enabled identification of 13 distinct cell clusters, including ISCs (stem), distinct populations of transitamplifying (TA) cells, goblet cells, EECs, tuft cells, and two types of colonocytes (Figures 1B and 1C; Table S2) (Parikh et al., 2019). Trajectory inference based on high-resolution clustering separated the cells into five major lineages (Figure 1D).

We next performed RNA velocity analysis to infer differentiation trajectories (Figures 1E and S1D). We observed a strong directionality originating at the ISC clusters, through distinct TA populations and into fully differenti-

ated cell types along all the five lineages (Figure 1E). TA populations, which included cells in S and G2/M phase, were found at the root of each trajectory (Figures 1E and S1E). Of note, the fraction of cells in S and G2/M was significantly higher in the TA clusters than in the ISC cluster (Figure S1F). This was supported by the observation that most dividing cells (phospho S10 histone H3-positive) are located above the ISC zone (Figures S1G and S1H) and suggests that TA populations may serve as the main source of tissue replenishment, as previously proposed (Ishikawa et al., 2022).

As expected, using immunofluorescence and spatial transcriptomics, the expression of the proliferation markers proliferating cell nuclear antigen (PCNA- protein) and *HMGB2* (mRNA) was detected mainly in the lower part of crypts, whereas *KRT20*, a colonocyte and goblet cell differentiation marker, was found at the crypt top (CT) (Figures 1F–1H and S1I). Interestingly, the proliferation marker PCNA was detected in both trifoil factor 3 (TFF3) keratin-positive (goblet cells) and TFF3-negative cells in tissue sections (Figure 1F). Similarly, spatial transcriptomics showed the expression of the proliferation-associated *HMGB2* in *MUC2*-positive cells (Figure 1G), altogether suggesting that cell type specification may already occur in proliferative TA cells.

Finally, we observed the formation of unique cell clusters at the apex of the goblet and the two colonocyte lineage trajectories (Figures 1B–1D). Spatial transcriptomics confirmed that cells expressing markers of these endpoint clusters (*CEACAM1* and (*Keratin 20 - KRT20*) are located at the CT facing the intestinal lumen (Figures 1H and 1I). These populations shared a common gene signature, likely reflecting their unique environment (Figures S1J and S1K).

#### Ulceration promotes changes in cell behavior

To outline how the patterns of cell fate decisions are affected in UC, we next delineated cellular relationships in the disease-affected samples. We profiled matched biopsies from both visibly inflamed parts and neighboring healthy margins of the sigmoid colon (Figures 2A and S1A–S1C). Tissue damage in the ulcerated regions was evident at the morphological level, with crypts undergoing remodeling and lacking a defined top layer, while the

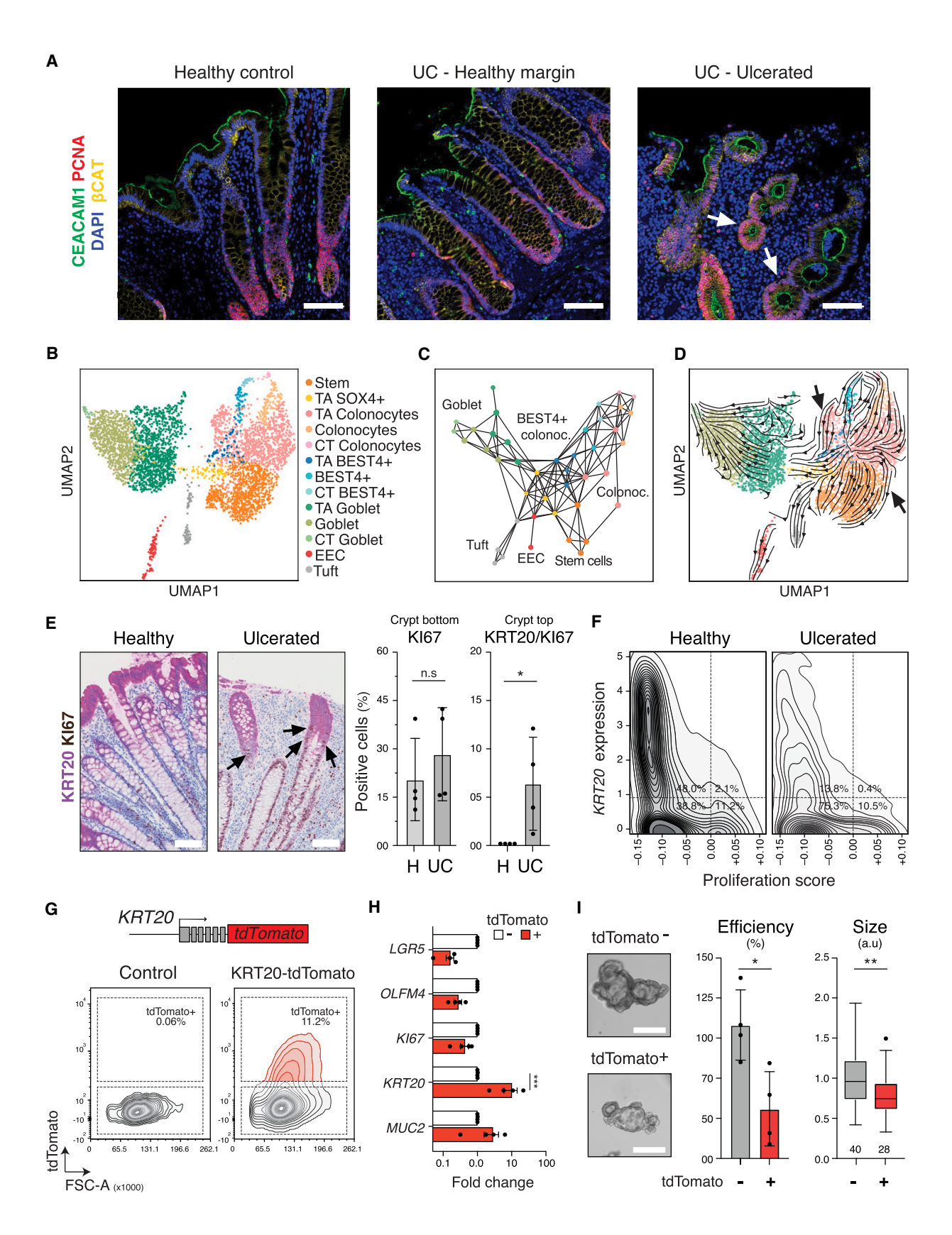
<sup>(</sup>D) Cell type trajectory graph based on over-clustering. Nodes represent clusters colored by cell type of origin, while connecting edges indicate the similarity degrees.

<sup>(</sup>E) RNA velocity measurements projected onto the UMAP embedding shown in (B).

<sup>(</sup>F) Immunostaining for TFF3 (blue), PCNA (red), and β-Catenin (green) in the healthy colonic epithelium. Arrow indicates a TFF3/PCNA double-positive cell. Scale bar: 100 μm.

<sup>(</sup>G–I) Spatial distribution of RNA molecules for MUC2 (red), HMGB2 (blue), KRT20 (orange), and CEACAM1 (green). DNA was counterstained with DAPI (gray). (G) and (H) show the entire crypts length. Scale bar: 50 μm. (I) shows a zoomed-in region of interest of crypt-top area. CT colonocyte (arrow) and goblet cell (arrowhead) are indicated. Scale bar: 10 μm (H).





(legend on next page)



epithelium from the adjacent healthy margins was morphologically similar to the healthy tissue (Figure 2A). Of note, the inflamed areas were associated with pronounced changes in cellular composition, with a higher proportion of CD45<sup>+</sup> immune cells and a lower fraction of EPCAM+ epithelial cells when compared to both the healthy samples and the matched healthy margins (Figures S1B and S1C).

To generate a map reflecting the cellular heterogeneity in patients with UC, we next compared the epithelial cells isolated from inflamed (4,351 cells) and healthy margin samples (6,762 cells). The same lineage-specific markers were used to define the cell type clusters and allowed the identification of the same cell populations in the patient-derived datasets (both ulcerated and healthy margins) as in the healthy dataset (Figures 2B and S2A-S2C). A deeper analysis of the datasets revealed substantial changes in the ulcerated regions (Figures 2C-2F). Firstly, trajectory analysis showed that the three most abundant cell lineages (classical and BEST4+ colonocytes and goblet cells) formed qualitatively less-defined branches, suggesting that common programs of epithelial differentiation might be disrupted in the ulcerated epithelium (Figures 2C, S2C, and S2D). Similarly, we observed reduced expression of the differentiation marker KRT20 in the ulcerated samples compared to non-ulcerated margin and healthy samples (Figure S3A). In addition, RNA velocity analysis indicated that normal differentiation patterns identified in the heathy samples were altered upon ulceration (Figure 2D). Notably, trajectories now existed into and out of the stem cell compartment (Figure 2D). In contrast, the expected patterns of differentiation were observed in the matched healthy margin dataset (Figures S2E and S2F).

Given the observations of dedifferentiation and developmental reprogramming events in experimental mouse colitis models (Yui et al., 2018), we speculated that differentiated cells could downregulate differentiation-associated transcriptional programs and reenter cell cycle in the human disease context. In agreement, the proliferative marker PCNA could be detected at upper levels of the crypts in ulcerated regions (Figure S3B). This was further supported by the detection of KRT20+ cells co-expressing the proliferation marker KI67 in ulcerated samples (Figure 2E). Importantly, more than 50% of the crypts analyzed contained double KRT20/KI67-positive cells, suggesting that this is a prevalent event in the ulcerated epithelium (Figure S3C).

Interestingly, we did not detect cells co-expressing high levels of *KRT20* and *KI67* in the scRNA-seq dataset, and cells with high *KRT20* expression had low proliferation scores in both healthy and ulcerated samples (Figure 2F). Given the long half-lives of keratins (Denk et al., 1987), we speculate that the detection of KRT20/KI67-double-positive cells at the protein level indicated that cells previously expressing KRT20 have reentered cell cycle while downregulating *KRT20* gene expression.

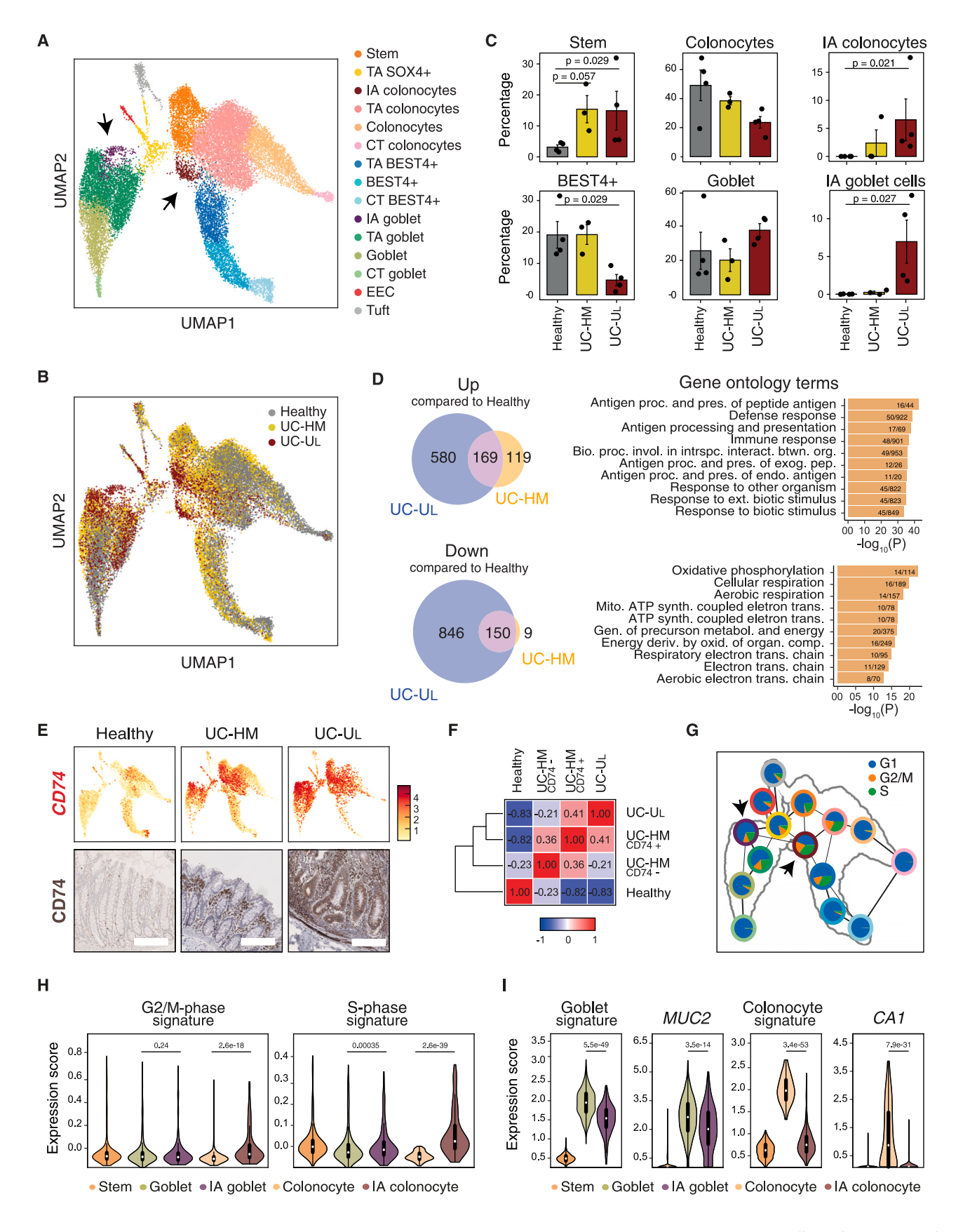
## Human colonic epithelial cells expressing the differentiation marker KRT20 display self-renewal potential *in vitro*

Based on the detection of KRT20/KI67-double-positive cells in the ulcerated epithelium, we hypothesized that KRT20-expressing cells retain latent ability to proliferate in

#### Figure 2. Altered cell fate patterns in the ulcerated epithelium samples

- (A) Immunostaining for CEACAM1 (green), PCNA (red), and β-catenin (yellow) human tissues. Scale bar: 100 μm.
- (B) UMAP depicting 4,351 colonic epithelial cells from patients with UC following cell type annotation as in (1B).
- (C and D) Trajectory graph based on over-clustering and RNA velocity analysis of epithelial cells from ulcerated samples. Arrows (D) point to velocity vectors going from differentiated cell clusters toward progenitor clusters.
- (E) (Left) representative image of immunohistochemistry staining for KRT20 and KI67 in healthy and ulcerated human colonic samples. Arrows indicate KRT20/KI67 double-positive cells. (Right) bar plots showing percentage of KI67 single-positive and KRT20/KI67 double-positive cells in the indicate areas. Each dot represents an individual donor (average of at least 5 crypts each). H, healthy controls; UC, ulcerated samples. \* for p < 0.05 by Student's t test. Scale bar:  $100 \mu m$ .
- (F) Density plots showing of KRT20 expression (y axis) and proliferation score (x axis) in the healthy (left) and ulcerated (right) datasets. (G) Representative flow cytometry analysis of KRT20-tdTomato human organoid reporter line. A wild-type line was used as a control for tdTomato levels. Schematic of the reporter gene is shown above.
- (H) Quantitative reverse-transcription PCR (RT-qPCR) analysis of the indicated genes in tdTomato<sup>-</sup> and tdTomato<sup>+</sup> sorted from KRT20-tdTomato reporter line. Expression levels of genes of interest were normalized to *GAPDH*. Bars show fold change relative to KRT20-tdTomato<sup>-</sup> cells  $\pm$ SEM; each dot represents an independent experiment. \*\*\* for p < 0.005 by ordinary 2-way AVOVA with Sidak's correction for multiple comparison.
- (I) (Left) representative phase-contrast images of human colon organoids formed from sorted tdTomato $^-$  and tdTomato $^+$  (bottom) cells 10 days after seeding. Scale bars: 275  $\mu$ m. (Right) quantification of organoid-forming efficiency and size of organoids formed from purified KRT20-tdTomato $^-$  and tdTomato $^+$  cells. For efficiency, plot shows mean  $\pm$  SEM; each dot represents an independent experiment (average of four replica per experiment). For size, plot was generated using the Tukey method. The number of organoids analyzed within one representative experiment is shown below the bars.







growth-permissive environments. To test this, we utilized a human colonic organoid reporter line with tdTomato introduced into the 3'UTR of the KRT20 locus (Shimokawa et al., 2017; Figure 2G). As expected, purified tdTomato-positive (KRT20+) cells expressed higher levels of differentiation markers (KRT20 and MUC2) and reduced levels of stem cell (LGR5 and OLFM4) and proliferation (KI67) markers compared to the tdTomato-negative (KRT20<sup>-</sup>) fraction (Figure 2H). We next assessed the self-renewal potential of tdTomato-positive and tdTomato-negative cells using organoid formation assay as an in vitro model of regeneration (Pikkupeura et al., 2023; Serra et al., 2019). Suggestive of latent self-renewal capacity, tdTomato-positive (KRT20+) cells could form organoids within seven days, although with reduced efficiency and size compared to tdTomatonegative (KRT20-) cells (Figure 2I). This supported the idea that cells expressing markers of differentiation possess regenerative properties in an injury-mimicking, growthpermissive environment.

#### Emergence of unique cellular states upon ulceration

Based on the findings that the cellular trajectories were altered in the ulcerated samples, we next integrated the three scRNAseq datasets (healthy, ulcerated, and healthy margin) to directly investigate changes in cellular complexity (Figures 3A, 3B, and S4). Cluster analysis revealed that the relative abundance of each cluster was altered in the inflamed and, to a lesser extent, adjacent healthy margin samples (Figures 3B and 3C). Interestingly,

ulcerated and healthy margin samples had an increased proportion of cells assigned to the ISC cluster (Figure 3C). In addition, cells within the ISC cluster in the patient-derived samples were transcriptionally distinct from those of the healthy samples (ulcerated vs. healthy: 749 up- and 996 downregulated genes; healthy margin vs. healthy: 288 up- and 159 downregulated genes; Log2FC>+/-0.5, p < 0.05; Figure 3D). Of note, we observed a significant overlap in differentially expressed genes in the patient samples when each is compared with the healthy ISC counterpart (up:  $p = 2.3 \times 10^{-142}$ ; down  $p = 2.4 \times 10^{-163}$ ). The shared upregulated genes in patient samples were enriched in Gene Ontology (GO) terms associated with interferon signaling and antigen processing, whereas shared downregulated genes were enriched for cellular respiration (Figure 3D).

In addition to cluster-specific changes, we also observed expression changes across various cell-type clusters in inflamed and adjacent healthy margin samples. Among those, CD74, an immune cell marker previously reported to be expressed in the colonic epithelium of IBD patients (Parikh et al., 2019), was detected at higher levels in the healthy margin and ulcerated samples (Figure 3E). In agreement, CD74 protein could also be observed in tissue from ulcerated regions and neighboring healthy margins (Figure 3E). Notably, using Pearson correlations, we observed that  $CD74^+$  cells in the healthy margins were more representative of the ulcerated dataset, whereas  $CD74^-$  cells represented an intermediate between the ulcerative and healthy state (Figure 3F). Altogether this

#### Figure 3. Emergence of new cell states in the ulcerated epithelium

- (A) UMAP of epithelial cells from the combined datasets from healthy individuals, and patient-derived healthy margin and ulcerated samples. Colors indicate different cell cluster types. Arrows indicate the inflammation-associated cell clusters.
- (B) UMAP of the combined datasets from healthy, healthy margin, and ulcerated epithelial cells colored by cell type and dataset of origin. (C) Bar plots showing cell fractions within the indicated lineages in the healthy, healthy margin, and ulcerated datasets, including the IA cell states. Colonocytes, BEST4+, and goblet cell lineages include TA and CT populations. Significance tested with two-sided Mann-Whitney U test. Each dot represents an individual donor. Bars represent the mean  $\pm$  SEM. UC-HM, UC patient-derived healthy margin; UC-UL, patient-derived ulcerated samples.
- (D) (Left) Venn diagrams indicating the number of shared upregulated and downregulated genes between the stem cell clusters from the ulcerated and healthy margin samples (when compared to the healthy state). (Right) bar plots showing top 10 terms from GO term overrepresentation analyses of the shared differentially expressed genes. Numbers in each bar indicate the fraction of genes within that GO term found in the shared differentially expressed genes (DEGs).
- (E) Analysis of CD74 expression in the indicated samples. (Top) UMAP plots with heatmaps of normalized expression of the *CD74* gene in the integrated dataset split by sample type of origin. (Bottom) Representative immunohistochemistry images for CD74 in tissue biopsies. Scale bars: 100 μm.
- (F) Similarity correlation matrix between healthy, ulcerated, and healthy margin samples. The last was split into CD74-positive and negative fractions (cutoff value based on the third quartile of CD74 expression in the healthy dataset). Similarity among samples calculated based on first 50 principal components using Pearson correlation. Dendrogram lines on the left shows hierarchical clustering of the sample types.
- (G) Trajectory graph of cell type clusters in the integrated datasets. Pie charts indicate proportions of cells in each cell-cycle phase. Outer ring colors match cell type clusters in (A).
- (H and I) Violin plots showing normalized enrichment score of the indicated signatures and expression levels of the indicated lineage-specific genes (*CA1* and *MUC2*) in the stem cell, IA colonocyte, and IA goblet clusters from the ulcerated samples. Significance was tested with two-sided Mann-Whitney U test.



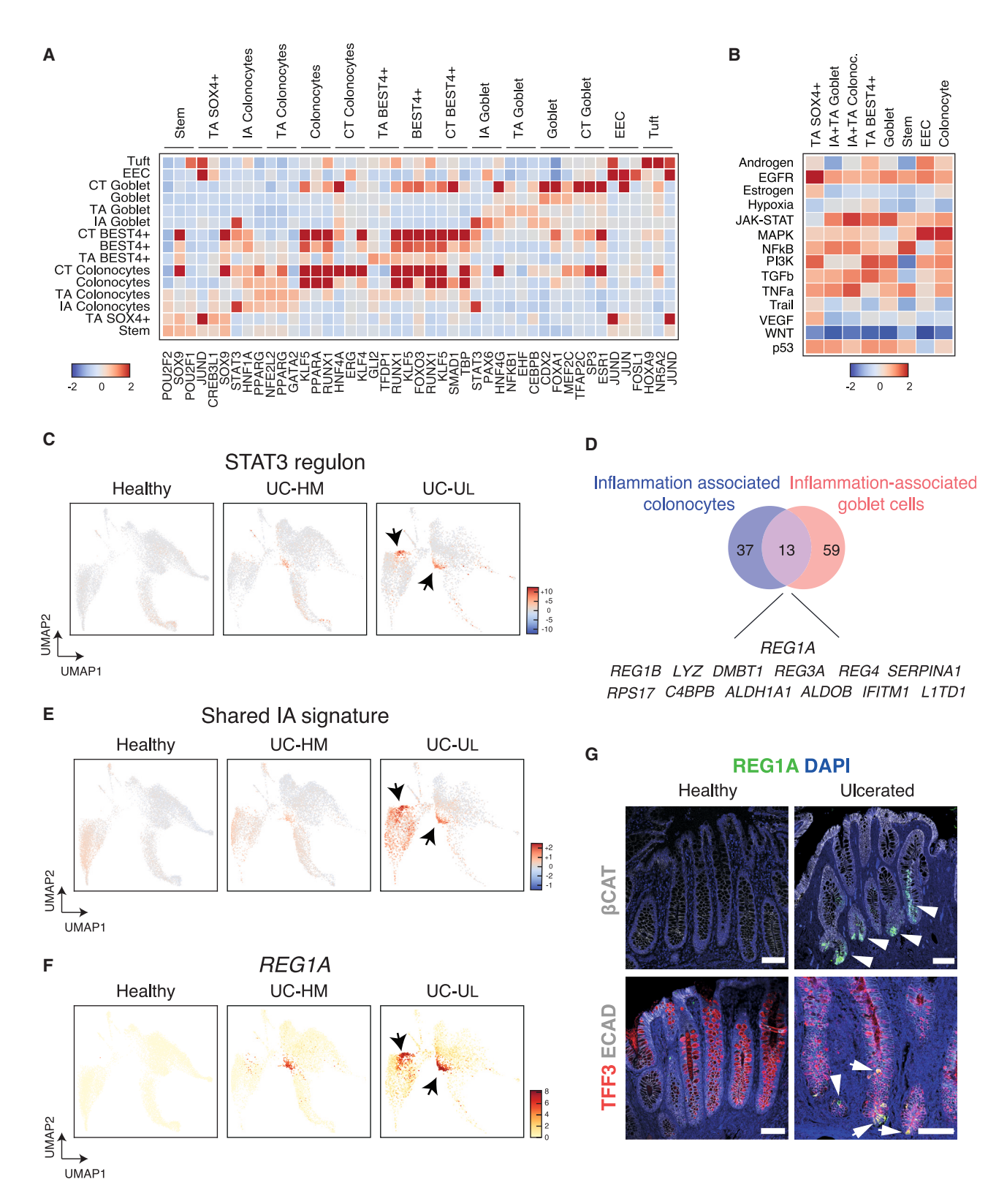


Figure 4. Inflammation-associated cell states are associated with JAK/STAT signaling

(A) Heatmap of scaled transcription factor activity from the annotated DoRothEA regulons. Top three differentially active regulons for each of the cell type clusters are depicted.

(legend continued on next page)



suggests that seemingly healthy areas were altered in patients with UC.

Finally, in the clustering analysis, we observed the emergence of two new cell populations assigned to the colonocyte and goblet cell lineages in ulcerated and, to a lesser extent, healthy margin samples (Figures 3A–3C). The two populations were only detected in epithelium of patients with UC and were accordingly named IA colonocytes and IA goblet cells. IA clusters were characterized by a high proportion of proliferating cells (Figures 3G, 3H, and S5A), and reduced expression of differentiation genes, including *KRT20*, compared to their respective non-IA colonocyte and goblet counterparts within the ulcerated samples (Figures 3I, S5B, and S5C).

IA cells clustered independently and were part of the reverse trajectories observed in the ulcerated dataset (Figures S5D and S5E). Of note, correlation analysis indicated that IA colonocytes and IA goblet cells were most similar to cells in their respective lineages and to each other (Figure S5F). This was unlike the other colonocyte and goblet cell clusters, which correlated only with their respective lineages. Highlighting the uniqueness of these populations, GO-term analysis of the differentially expressed genes in the IA goblet cells and IA colonocytes showed enrichment in cytokine and interferon signaling, immune response, and antigen processing, similar to what was observed for the ISC compartment (Figures S5G and S5H). Altogether, these data suggested that the new IA clusters contained cells in a proliferative state that were linked with signals originating from the immune system.

#### Emergence of IA cellular states is associated with JAK/ STAT activation

We next utilized DoRothEA, a collection of transcription factor (TF) and target gene interactions (Garcia-Alonso et al., 2019), to infer which gene regulatory networks (GRNs) were associated with the IA cell populations. Aligned with the enrichment of GO terms associated with cytokine and interferon signaling (Figures S5G and S5H), the analysis identified STAT3 as the most enriched GRN

at the single-cell and population level (Figures 4A–4C; Table S3;  $p < 10^{-100}$ ).

To further investigate the features of the IA cell states, we examined genes uniquely expressed by the two populations when compared to respective goblet and colonocyte lineages. Less than 100 genes were found to be differentially expressed in each population, and 13 of them were shared between the two IA populations. These included several reported STAT target genes, such as REG1A, REG1B, REG3A, DMBT1, ALDH1A1, C4BPB, and IFITM1 (Figures 4D-4F). Notably, REG1A (Regenerating Family Member 1 alpha) was identified as unique to the two IA cell states and expressed across the entire cell populations. Examination of an independent dataset (Parikh et al., 2019) confirmed the unique expression of REG1A in subsets of cells in samples from patients with UC (Figure S6A). At the protein level, REG1A was detected in ulcerated epithelium in both TFF3+ and TFF3- cells, supporting the emergence of these cell states in the goblet cell and colonocyte lineages (Figure 4G). Altogether, the data revealed that unique cellular states exist in the ulcerated epithelium characterized by active cell cycle and a transcriptional signature associated with cytokine and STAT signaling.

### JAK/STAT activation by IL-22 increases regenerative properties in human colonic organoid cultures

The JAK/STAT signaling pathway mediates inflammatory and proliferative responses downstream of cytokine stimulation (Philips et al., 2022). Interleukin-22 (IL-22) is one of several cytokines that activates STAT signaling and has been implicated in tissue repair following intestinal damage in murine models (Cox et al., 2021; Lindemans et al., 2015). To investigate how STAT activation affected the human colonic epithelium, we resorted to organoid cultures derived from healthy individuals. These were treated with IL-22, and, analogous to the transcriptional changes observed *in vivo*, the differentiation marker *KRT20* was downregulated and IA signature genes were upregulated (*REG1A*, *DMBT1*, and *REG3A*; Figures 5A–5C). Treatment with a pan-JAK inhibitor (tofacitinib) could block these changes, confirming the specific involvement of

<sup>(</sup>B) Heatmap of scaled pathway activity for ulcerated cell populations. Activity scores have been calculated using genes differentially expressed in the ulcerated dataset, as compared to the healthy dataset. The DEGs have been found between pseudo-bulk profiles of cell types from the two datasets when at least two biological replicates per condition were available. In the ulcerated dataset, IA Colonocytes and IA goblet cells have been combined with TA colonocytes and TA goblet cells, respectively.

<sup>(</sup>C) UMAP plot showing enrichment for STAT3 transcriptional regulon in the integrated dataset split by sample type. Arrows indicate location of IA clusters in the ulcerated samples.

<sup>(</sup>D) Venn diagram of the intersection between shared upregulated genes in IA colonocytes and IA goblet cells (compared to their respective lineages) in the ulcerated dataset.

<sup>(</sup>E and F) UMAPs with a heatmap of the normalized thirteen IA signature genes (E) and REG1A expression in as in (C).

<sup>(</sup>G) Representative immunofluorescent images for REG1A (green), TFF3 (red), and b-catenin or E-Cadherin (white) in healthy and ulcerated tissue samples. Arrowheads indicate single REG1A-positive cells. Arrows indicate TFF3/REG1A double-positive cells. Scale bars: 100 μm.



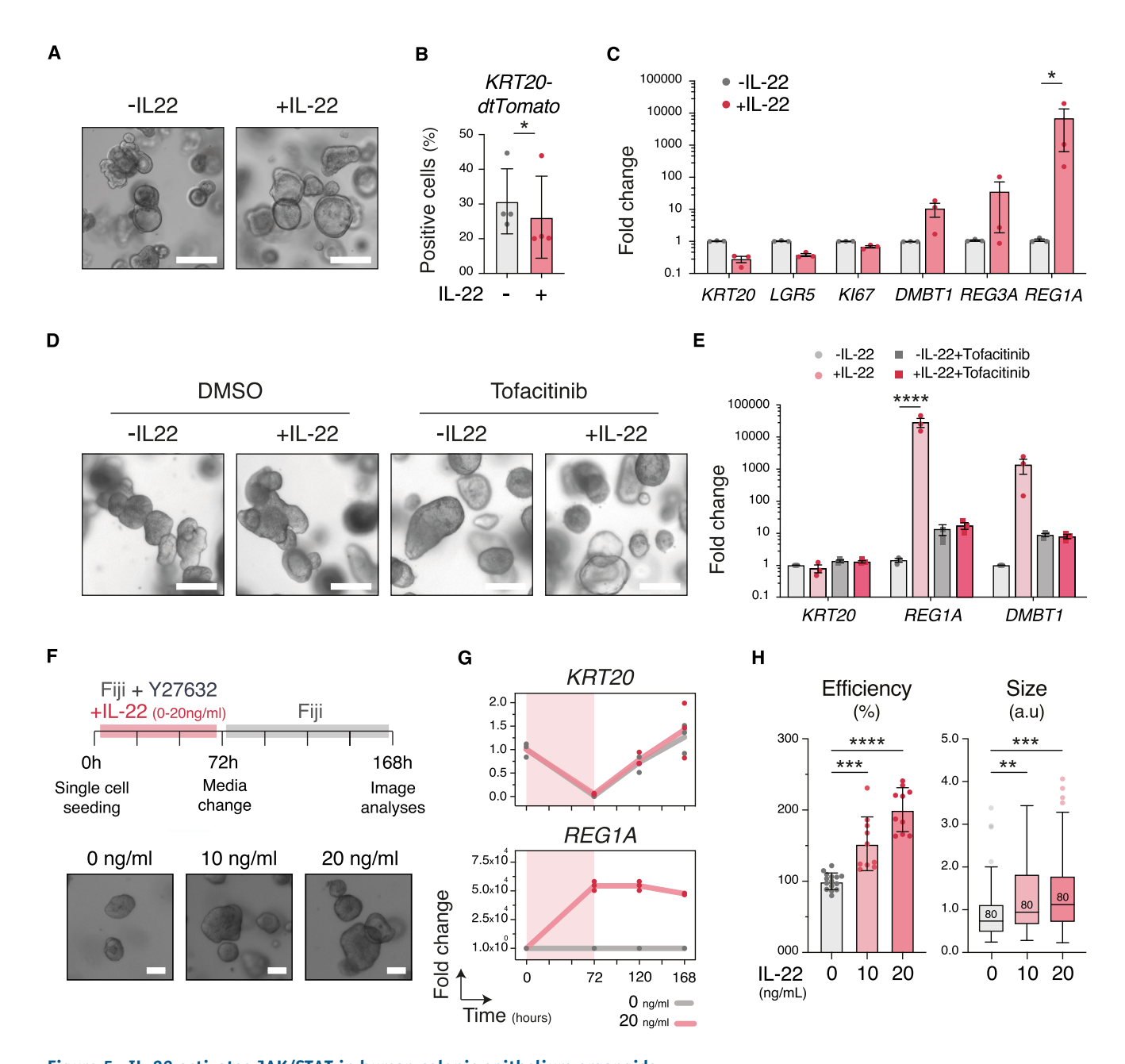


Figure 5. IL-22 activates JAK/STAT in human colonic epithelium organoids

- (A) Bright-field images of control and IL-22-treated human colonic organoids for 3 days. Scale bars: 200 µm.
- (B) Bar plot showing reduction of tdTomato+ cells (KRT20-tdTomato reporter line) following treatment with IL-22. Each dot represents an independent experiment (average of 3–6 replica wells per experiment). \*p < 0.05 by paired Student's t test.
- (C) RT-qPCR analysis showing relative expression levels of indicated genes following IL-22 treatment. Plot shows fold change relative to untreated organoids  $\pm$  SEM. Each dot represents an independent experiment. \*p < 0.5 by two-way ANOVA.
- (D) Representative images of human colonic organoids with IL-22 and/or JAK inhibitor tofacitinib for 3 days. Scale bars, 200 μm.
- (E) RT-qPCR analysis of showing relative expression of the IA-associated genes following treatment with IL-22 and/or tofacitinib as in (D). Plot depicts fold change relative to untreated control organoids  $\pm$ SEM; each dot represents an independent experiment. \*\*\*\* for p < 0.001 by paired two-way ANOVA followed by Dunnett's multiple comparison test.
- (F) Schematics of organoid formation assay setup. Bottom part shows representative images of organoids at 168 h formed following treatment with with IL-22 at the indicated concentrations during the initial 72 h.
- (G) Time course RT-qPCR analysis confirming upregulation of REG1A upon IL-22 treatment. Pink shade indicates exposure window to IL-22. Each dot represents technical replicas of a single representative experiment.

(legend continued on next page)



JAK/STAT signaling (Figures 5D and 5E). Of note, the response was not affected by inhibition of mammalian target if rapamycin (mTOR) signaling, which has been shown to mediate IL-22-induced Paneth cell differentiation (He et al., 2022; Figures S6B-S6D).

To functionally test the effect of JAK/STAT activation on regenerative properties, we treated single cells isolated from organoids with IL-22 during the initial 72 h (Figure 5F). Indeed, IL-22 exposure led to robust upregulation of REG1A and significantly augmented organoid formation efficiency and organoid size (Figures 5G and 5H). Finally, in the KRT20-tdTomato reporter line, exposure to IL-22 during the initial 72 h specifically enhanced the organoid-forming capacity of the KRT20-tdTomato+ population (Figures S6E and S6F). In summary, these results indicate that IL-22 triggered changes observed in the ulcerated epithelium and that activation of JAK/STAT was associated with increased regenerative properties of colonic epithelial cells in vitro.

#### Cytokine-induced JAK/STAT signaling is sufficient to promote IA cell states

To address whether IL-22 signaling was sufficient to promote the emergence of the IA cell states, we performed scRNA-seq on three independent human colonic organoid lines cultured with or without IL-22 (Figures 6A and S7A). Except for BEST4+ colonocytes, all major cell populations could be identified in the untreated samples. Importantly, IL-22-treated samples also contained cell clusters that transcriptionally matched the IA states identified in the UC datasets (Figure 6A). Analogous to the patient data, these new clusters belonged to the goblet cell and colonocyte compartments and showed increased expression of STAT3 regulon as well as IA signature genes (including REG1A) (Figures 6B-6D). In addition, as observed in the patient dataset, IA colonocytes and goblet cells showed reduced expression of their respective lineage differentiation genes, when compared to their non-IA counterparts (Figures 6E and 6F).

To assess the regenerative capacity of the IA populations, we engineered a REG1A reporter line by fusing a mNeonGreen (mNeon) tag to the C terminus of REG1A via CRISPR-Cas9 editing (Figures 6G and S7B). Two independent clonal lines were derived and, upon IL-22 treatment, showed levels of REG1A induction comparable to the observed in the scRNA-seq dataset (approximate 15% REG1A-mNeon+cells; Figures 6H and S7C-S7E). Treatment with JAK or mTOR inhibitors further confirmed that

REG1A expression was regulated through the JAK/STAT pathway (Figures 6I and S7F). Using the reporter lines, we also confirmed that REG1A expression was specifically induced by IL-22, and not by other cytokines activating JAK/STAT signaling (IL-13, interferon [IFN]-γ and tumor necrosis factor alpha [TNF- $\alpha$ ]; Figure S7G).

Finally, to characterize the properties of the REG1A-expressing cells, we purified mNeon- and mNeon+ cells by flow cytometry and performed organoid formation assay. As expected, mNeon+ cells showed reduced expression of KRT20 and increased expression of IA genes (REG1A, REG3A, and DMBT1; Figures 6J and S7H). To a lesser extent, these genes followed the same trend in the mNeon- cells from the IL-22-treated cultures when compared to the non-treated (mNeon-) cells (Figures 6J and S7H).

In terms of organoid formation, mNeon- and mNeon+ cells both formed organoids at a similar efficiency, demonstrating that the cytokine-induced REG1A-expressing cells retain the capacity to self-renewal. Suggestive of increased regenerative properties, mNeon+ cells, however, formed significantly larger organoids than those formed from mNeon- cells, from either previously IL-22-treated or untreated cultures (Figures 6K and S7I). Altogether, these results demonstrated that human colonic organoid cultures recapitulate key aspects of the IA cell populations and allow functional assessment of their regenerative properties in vitro.

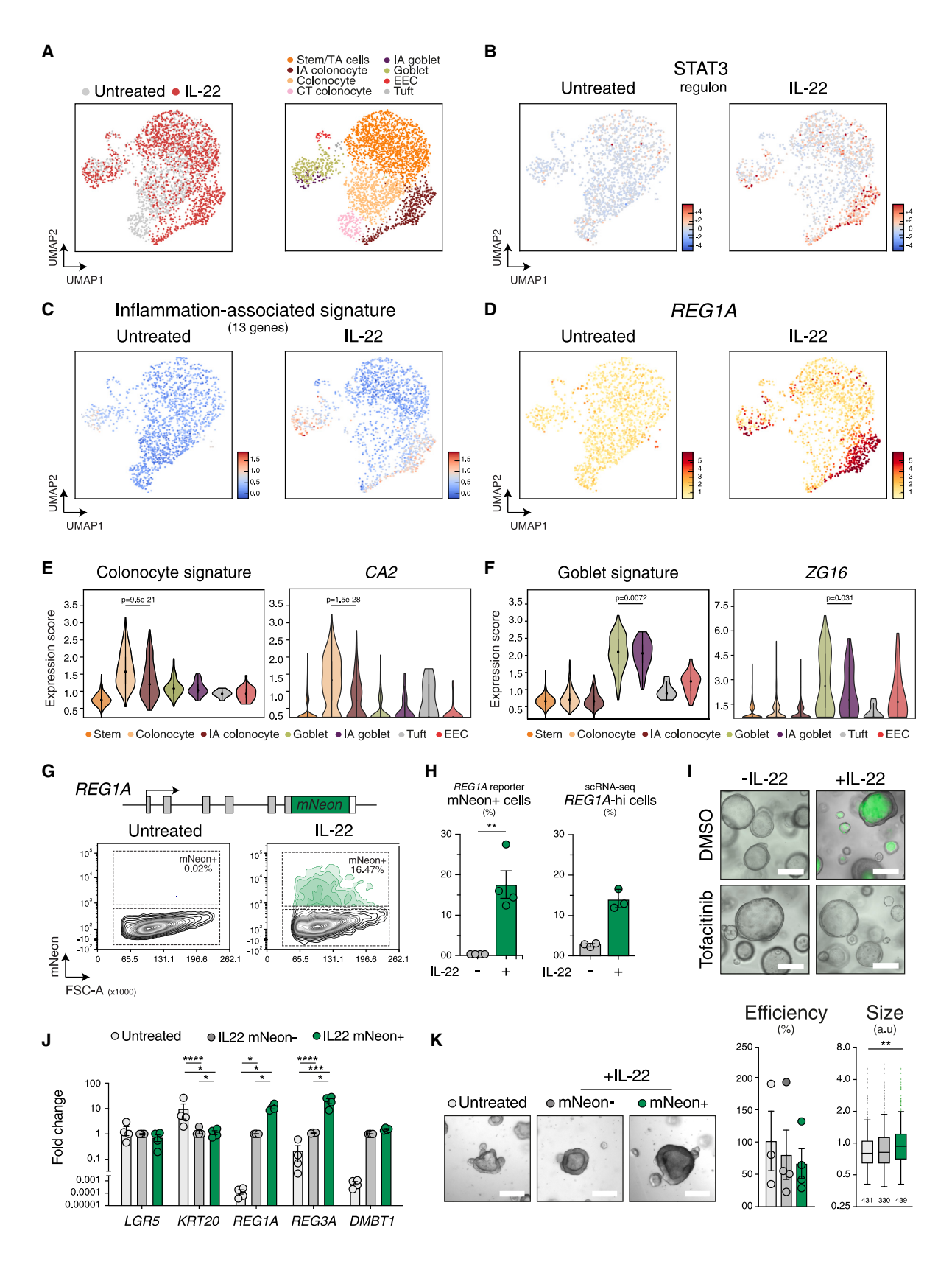
#### Inhibition of JAK/STAT signaling impairs functional recovery in mouse colitis model

To assess the effect of JAK/STAT signaling on tissue repair in vivo, we assessed the impact of pathway inhibition on tissue regeneration using the dextran sulfate sodium (DSS)induced colitis model (Figure 7A). Following the treatment with DSS in drinking water, mice were treated with the pan-JAK inhibitor, tofacitinib, during the early repair phase. In agreement with the role of JAK/STAT in regeneration, tofacitinib-treated animals developed more severe colonic damage and greater weight loss, when compared to vehicle-treated animals (Figures 7A–7C). Thus, as described for STAT3 (Oshima et al., 2019), we speculate that JAK signaling is required for initiating epithelial regeneration in vivo.

In summary, we demonstrate that ulceration alters population dynamics in the colonic epithelium. Our data suggest that these changes are regulated by intricate relationships between the epithelial cells and cytokine signals, which play an important role in epithelial tissue

<sup>(</sup>H) Quantification of organoid forming efficiency and organoid size following IL-22 treatment as indicated in (F). For efficiency, plot shows mean ± SD. Each dot represents a replica well of three independent experiments. For size, plot was generated using the Tukey method. The number of organoids analyzed within one representative experiment is shown below the bars. a.u, arbitrary unit. \*\*, \*\*\*, and \*\*\* for p < 0.01, 0.005, and 0.001, respectively, by two-way ANOVA.





(legend on next page)



regeneration. Although we cannot formally prove with the currently available tools and datasets, our findings corroborate the idea of injury-induced changes in cellular identity as a key element of tissue regeneration (Larsen and Jensen, 2021).

#### **DISCUSSION**

Here, we present a comprehensive analysis of the healthy and ulcerated colonic epithelium from patients with UC. Our analyses indicate that, in steady-state conditions, lineage choices may occur in early lineage-biased TA populations and follow a unidirectional, forward differentiation pattern. This unidirectional flow of cells from the stem and TA compartments appears, however, perturbed in the ulcerated epithelium, as observed in mouse models of injury (Tetteh et al., 2016; van Es et al., 2012). Such changes in cellular behavior could be recapitulated in genetically engineered human organoid lines, wherein cells expressing markers of differentiation were capable of self-renewing in injury-mimicking and growth-permissive environments.

Activation of developmental pathways appears to be a common mechanism of intestinal epithelial regeneration (Meyer et al., 2022). In experimental models of acute injury, regenerative responses entail loss of markers associated with adult stem and terminally differentiated cells, as well as the emergence of cells phenotypically analogous to fetal epithelial progenitors (Nusse et al., 2018; Yui et al., 2018). Interestingly, in samples from patients with UC, we observed, both in the colonocyte and goblet cell lineages, the appearance of

new cell states characterized by increased proliferative scores and reduced expression of lineage-specific genes. *In vitro*, these cellular states could be recapitulated by stimulation with the pro-inflammatory cytokine IL-22 and allowed the assessment of the regenerative potential of cells with these features. Despite the technical inability to formally prove their contribution *in vivo*, the identification of these common features—i.e., loss of differentiation, increased proliferation, and gain in self-renewal ability—indicates that developmental resetting events might also occur in human chronic disease contexts. It remains to be investigated whether similar events occur in other chronic acute injury contexts, such as Crohn's disease and  $\gamma$ -radiation-induced injury, and how these responses are temporally regulated following tissue damage.

Transcriptionally, the IA cell states were characterized by a strong enrichment of STAT target genes, a feature that has previously been linked to tissue regeneration (Pickert et al., 2009; Taniguchi et al., 2015). This was further supported by *in vitro* experiments, in which treatment with IL-22, a secreted factor that activate JAK/STAT signaling (Lindemans et al., 2015; Pickert et al., 2009), led to the emergence of the IA states within both the goblet and colonocyte branches. Of note, we identified the STAT target *REG1A* as a diagnostic marker of the IA states. This is aligned with studies in mice, in which *Ly6a* (Sca1), another STAT target gene without known homologs in human, is associated with the emergence of cells involved in tissue regeneration (Yui et al., 2018; Nusse et al., 2018; Rao et al., 2015).

#### Figure 6. IL-22 treatment recapitulates the emergence of IA cellular states in human colonic organoids

- (A) UMAP plots of control and IL-22-treated organoid datasets colored by condition (left) and cell type annotation (right).
- (B and C) UMAP plots showing enrichment for STAT3 transcriptional regulon (C) and the shared IA signature (C) in control and IL-22-treated organoids.
- (D) UMAP plots with a heatmap of normalized expression REG1A in control and IL-22-treated organoids.
- (E and F) Violin plots showing normalized enrichment score of the indicated signatures and expression levels of the indicated lineage-specific genes (CA2 and ZG16) in the cell type clusters identified in organoids treated with IL-22.
- (G) Representative flow cytometry analysis of REG1A-mNeon human organoid reporter line (clone#3) following IL-22 treatment for 3 days. Simplified schematic of the reporter is shown above.
- (H) Quantification of REG1A-expressing cells in human colonic organoids treated with IL-22. Bar plots showing percentage of mNeon-positive cells (mean  $\pm$  SD) in the REG1A-mNeon reporter line (clone#3; left) and percentage of high REG1A cells (normalized expression in the third quantile) in the scRNA-seq dataset (right). Each dot represents an independent experiment. \*\* by paired Student's t test.
- (I) Representative images of REG1A-mNeon reporter line (clone#3) treated with IL-22 and/or tofacitinib for 3 days. Images show merged phase contrast and GFP channels. The secreted REG1A-mNeon fusion protein accumulates in the lumen of the organoids. Scale bars: 200 µm.
- (J) RT-qPCR analysis showing relative expression levels of the indicated genes in the fluorescence-activated cell sorting (FACS)-purified cell populations from the REG1A-mNeon reporter line (clone#3). Fold change relative to mNeon— cells  $\pm$ SEM. Each dot represents an independent experiment. \*p < 0.05, \*\*p < 0.01, \*\*\*\*p < 0.001, \*\*\*\*\*p < 0.0001; two-way ANOVA with Tukey's multiple comparison test. (K) Organoid-forming assay of purified mNeon-negative and mNeon-positive cells from IL-22-treated organoids (clone#3). mNeon-negative cells from untreated organoids were used as control. Left shows representative images of organoids formed from each purified cell fraction. Scale bar: 300  $\mu$ m. Right shows quantification of formation efficiency and organoid size, as described in (21). Efficiency plot shows mean  $\pm$  SEM. Each dot represents an independent experiment. Size is shown as Tukey plot in log2 scale. The number of organoids analyzed within one representative experiment is shown below the bars. \*\* for p < 0.01 by one-way ANOVA.



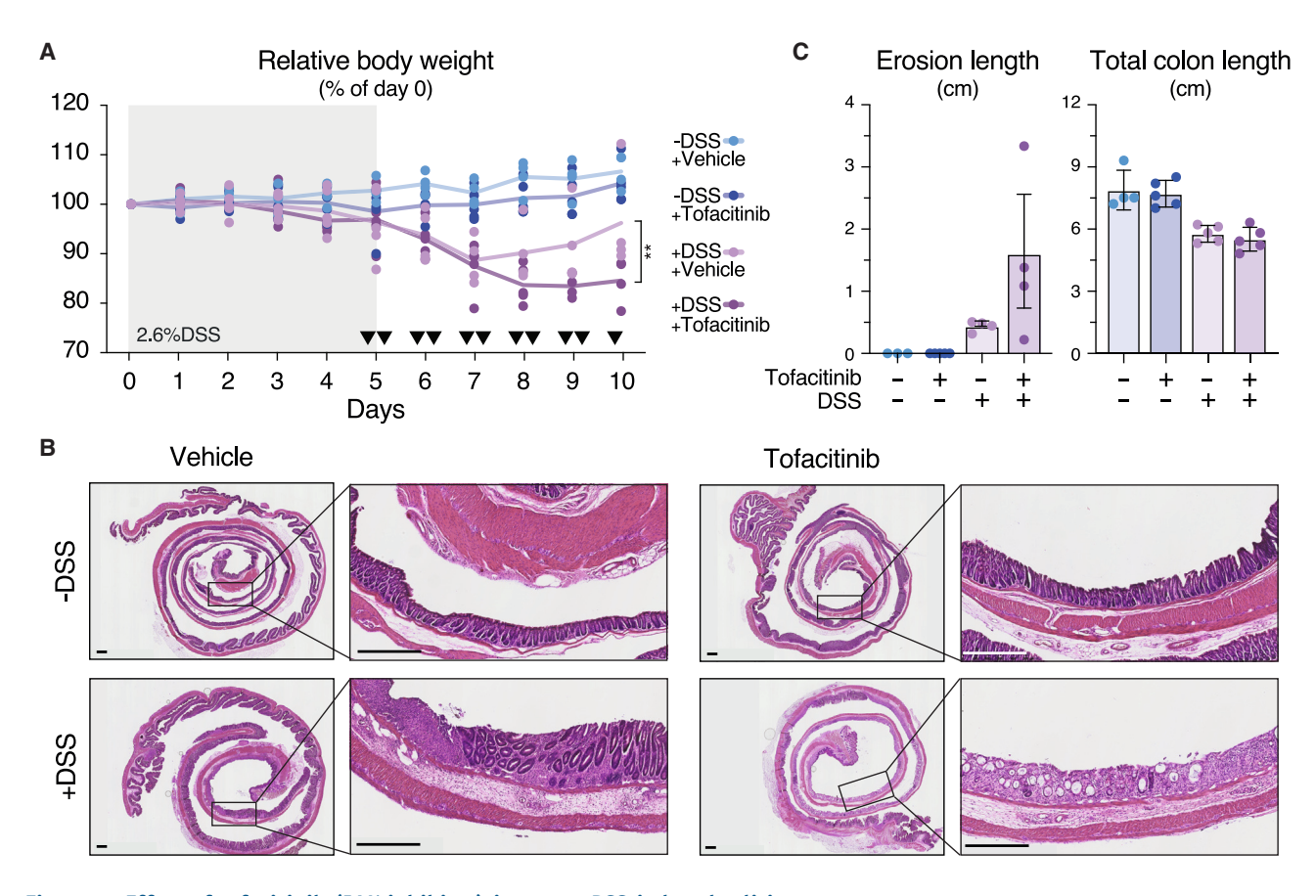


Figure 7. Effect of tofacitinib (JAK inhibitor) in mouse DSS-induced colitis

(A) Time course analysis of body weight changes of mice in all experimental groups. Gray shade (from day 0 to day 5) indicates presence of DSS in drinking water. Arrow heads indicate doses of vehicle or tofacitinib. Individual dots represent the relative weigh of each animal compared to day 0. \*\* for p < 0.01 at day 10 by two-way ANOVA followed by Šídák's multiple comparisons test.

- (B) Swiss roll sections of colon from control and DSS groups as indicated in (A). Sections were stained with hematoxylin & eosin (H&E). Scale bar: 600 μm.
- (C) Assessment of tissue damage in the histological preparations. Left plot shows length of epithelial erosions from H&E staining. Right plot shows total length of the colon for comparison. Individual dots represent the values for individual animals at day 10.

Using experimental colitis model, we also provide evidence that JAK signaling is required for efficient tissue recovery. Our data suggest that, in addition to promoting the inflammatory process, JAK signaling might be important for the regenerative response within the epithelium. Given the observed clinical benefits of pan-JAK inhibitors in patients with IBDs (Honap et al., 2024), it is likely that their immunosuppressive effects outweigh the effects on epithelial recovery. Nonetheless, it would be of importance to further dissect the immune-mediated and direct effects of JAK inhibition on epithelial recovery, and whether these could be disentangled with the availability of novel selective JAK inhibitors currently under development (Honap et al., 2024).

Besides JAK/STAT, studies using mouse model of acute severe injury have also implicated WNT and yes-associated protein 1 (YAP-1) signaling in the process of epithe-

lial healing following tissue damage (Gregorieff et al., 2015; Harnack et al., 2019; Yui et al., 2018). Whether these signaling pathways are implicated in tissue regeneration in human chronic disease remains an open question. Larger cohort of patient samples and analyses of acute injury conditions might help shed light on the involvement of these signaling pathways in different types, severity, and/or phases of tissue repair in humans.

Collectively, we have investigated cell behavior in the ulcerated human colonic epithelium at high resolution using scRNA-seq and human organoid models. Our data highlight that colonic ulceration in humans is associated with pronounced changes in cellular identity and that this is driven via crosstalk between immune signals and epithelial cells. A deeper understanding of general mechanisms that regulate tissue regeneration will be important for the development of targeted treatment of UC. From a



therapeutic perspective, promoting a faster and more potent induction of regenerative state will launch new possibilities for more efficient mucosal healing in patients with UC and potentially complement current treatment strategies.

#### **EXPERIMENTAL PROCEDURES**

For additional information see supplemental experimental procedures.

#### Resource availability

#### Lead contact

Further information and requests for resources and reagents should be directed to and will be fulfilled by Kim Bak Jensen (kim.jensen@sund.ku.dk).

#### Materials availability

A completed Materials Transfer Agreement may be required for requested material.

#### Data and code availability

scRNA-seq data generated for this paper have been deposited at the European Genome-phenome Archive (EGA) repository and are publicly available as of the date of publication under the accession number EGAS00001007098.

#### **Human samples**

The study was approved by the Scientific Ethics Committee of the Capital Region of Denmark, filed under the ethical permission number H-18005342. All individuals provided written informed consent to participate in this study. Participants were informed both orally and in writing in compliance with the Declaration of Helsinki and the guidelines of the Danish National Scientific Ethics Committee.

#### Single-cell expression profiling

Single-cell libraries from sorted cells were prepared using the  $10\times$  Genomics protocols and analyzed using established methodology. See supplemental experimental procedures for details.

#### **Human organoids**

Human organoid lines were established from the colonic epithelium of three healthy donors and maintained as described in the supplemental experimental procedures.

#### **Animal experiments**

All animal experiments and procedures were conducted in accordance with the recommendations of the European Community Directive (2010/63/EU) and approved by the Danish Animal Experiments Inspectorate under the license number 2017-15-0201-01381.

#### Statistical methods

Non-parametric t tests were used for the comparison between two different conditions. For experiments with more than two conditions, ANOVA test was used to calculate significance.

#### SUPPLEMENTAL INFORMATION

Supplemental information can be found online at https://doi.org/10.1016/j.stemcr.2024.06.006.

#### **ACKNOWLEDGMENTS**

We thank Hans Clevers, Calvin Kuo, and Chris Garcia for kindly sharing cell culture reagents and plasmids; members of the Jensen and Nielsen labs and Viktor Petukhov for suggestions; and the reNEW Platforms and BRIC imaging and histology core for technical expertise and support. We further thank the staff at the Endoscopy Unit, Department of Gastroenterology and Department of Pathology, Herlev Hospital, for assistance with handling of patient tissue samples. The graphical abstract was created using BioRender. K.K. and A.M.B. are recipients of fellowships from the Copenhagen Bioscience Ph.D. Programme (NNF18CC0033666) and Danish Diabetes Academy (NNF17SA0031406). This work was supported by the Independent Research Fund Denmark (0134-00111B to K.B.J.), the Novo Nordisk Foundation (NNF17OC0028730, NNF18OC0034066, and NNF20OC0064376 to K.B.J.), the Leo Pharma Foundation (LF-OC-19-000169), and the European Union's Horizon 2020 research and innovation programme (STEMHEALTH ERCCoG682665 to K.B.J.). The Novo Nordisk Foundation Center for Stem Cell Medicine is supported by the Novo Nordisk Foundation (NNF21CC0073729).

#### **AUTHOR CONTRIBUTIONS**

O.H.N. and K.B.J. conceived the project. G.M., S.L.H., K. Krizic, L.K., R.B.B., S.U., M.M., A.M.B., T.S., O.H.N., and K.B.J. designed the experiments. L.K., L.B.R., and O.H.N. collected and analyzed the clinical samples. G.M., S.L.H., K. Krizic, L.K., R.B.B., M.J.I.Z., S.U., M.M., and A.M.B. performed the experiments. G.M. analyzed the scRNA-seq data. K. Khodosevich assisted with the scRNA-seq analyses. K.B.J. and R.B.B. wrote the manuscript with input from G.M., S.L.H., K. Krizic, L.K., and O.H.N. O.H.N. and K.B.J. contributed to funding acquisition. O.H.N. and K.B.J. supervised the study.

#### **DECLARATION OF INTERESTS**

T.S. is an inventor on several patents related to organoids.

Received: August 23, 2023 Revised: June 18, 2024 Accepted: June 19, 2024 Published: July 18, 2024

#### **REFERENCES**

Beumer, J., and Clevers, H. (2021). Cell fate specification and differentiation in the adult mammalian intestine. Nat. Rev. Mol. Cell Biol. *22*, 39–53. https://doi.org/10.1038/s41580-020-0278-0.

Cox, C.B., Storm, E.E., Kapoor, V.N., Chavarria-Smith, J., Lin, D.L., Wang, L., Li, Y., Kljavin, N., Ota, N., Bainbridge, T.W., et al. (2021). IL-1R1-dependent signaling coordinates epithelial regeneration in response to intestinal damage. Sci. Immunol. *6*, eabe8856. https://doi.org/10.1126/sciimmunol.abe8856.



de Sousa E Melo, F., and de Sauvage, F.J. (2019). Cellular plasticity in intestinal homeostasis and disease. Cell Stem Cell *24*, 54–64. https://doi.org/10.1016/j.stem.2018.11.019.

Denk, H., Lackinger, E., Zatloukal, K., and Franke, W.W. (1987). Turnover of cytokeratin polypeptides in mouse hepatocytes. Exp. Cell Res. *173*, 137–143. https://doi.org/10.1016/0014-4827(87) 90339-9.

Elmentaite, R., Ross, A.D.B., Roberts, K., James, K.R., Ortmann, D., Gomes, T., Nayak, K., Tuck, L., Pritchard, S., Bayraktar, O.A., et al. (2020). Single-cell sequencing of developing human gut reveals transcriptional links to childhood crohn's disease. Dev. Cell *55*, 771–783.e5. https://doi.org/10.1016/j.devcel.2020.11.010.

Fawkner-Corbett, D., Antanaviciute, A., Parikh, K., Jagielowicz, M., Gerós, A.S., Gupta, T., Ashley, N., Khamis, D., Fowler, D., Morrissey, E., et al. (2021). Spatiotemporal analysis of human intestinal development at single-cell resolution. Cell *184*, 810–826.e23. https://doi.org/10.1016/j.cell.2020.12.016.

Garcia-Alonso, L., Holland, C.H., Ibrahim, M.M., Turei, D., and Saez-Rodriguez, J. (2019). Benchmark and integration of resources for the estimation of human transcription factor activities. Genome Res. *29*, 1363–1375. https://doi.org/10.1101/gr. 240663.118.

Gehart, H., and Clevers, H. (2019). Tales from the crypt: new insights into intestinal stem cells. Nat. Rev. Gastroenterol. Hepatol. *16*, 19–34. https://doi.org/10.1038/s41575-018-0081-y.

Graham, D.B., and Xavier, R.J. (2020). Pathway paradigms revealed from the genetics of inflammatory bowel disease. Nature *578*, 527–539. https://doi.org/10.1038/s41586-020-2025-2.

Gregorieff, A., Liu, Y., Inanlou, M.R., Khomchuk, Y., and Wrana, J.L. (2015). Yap-dependent reprogramming of Lgr5(+) stem cells drives intestinal regeneration and cancer. Nature *526*, 715–718. https://doi.org/10.1038/nature15382.

Harnack, C., Berger, H., Antanaviciute, A., Vidal, R., Sauer, S., Simmons, A., Meyer, T.F., and Sigal, M. (2019). R-spondin 3 promotes stem cell recovery and epithelial regeneration in the colon. Nat. Commun. *10*, 4368. https://doi.org/10.1038/s41467-019-12349-5.

He, G.W., Lin, L., DeMartino, J., Zheng, X., Staliarova, N., Dayton, T., Begthel, H., van de Wetering, W.J., Bodewes, E., van Zon, J., et al. (2022). Optimized human intestinal organoid model reveals interleukin-22-dependency of paneth cell formation. Cell Stem Cell *29*, 1333–1345.e6. https://doi.org/10.1016/j.stem.2022.08.002.

Honap, S., Agorogianni, A., Colwill, M.J., Mehta, S.K., Donovan, F., Pollok, R., Poullis, A., and Patel, K. (2024). JAK inhibitors for inflammatory bowel disease: recent advances. Frontline Gastroenterol. *15*, 59–69. https://doi.org/10.1136/flgastro-2023-102400.

Ishikawa, K., Sugimoto, S., Oda, M., Fujii, M., Takahashi, S., Ohta, Y., Takano, A., Ishimaru, K., Matano, M., Yoshida, K., et al. (2022). Identification of quiescent LGR5(+) stem cells in the human colon. Gastroenterology *163*, 1391–1406.e24. https://doi.org/10.1053/j.gastro.2022.07.081.

Kinchen, J., Chen, H.H., Parikh, K., Antanaviciute, A., Jagielowicz, M., Fawkner-Corbett, D., Ashley, N., Cubitt, L., Mellado-Gomez, E., Attar, M., et al. (2018). Structural remodeling of the human colonic

mesenchyme in inflammatory bowel disease. Cell *175*, 372–386.e17. https://doi.org/10.1016/j.cell.2018.08.067.

Larsen, H.L., and Jensen, K.B. (2021). Reprogramming cellular identity during intestinal regeneration. Curr. Opin. Genet. Dev. 70, 40–47. https://doi.org/10.1016/j.gde.2021.05.005.

Le Berre, C., Honap, S., and Peyrin-Biroulet, L. (2023). Ulcerative colitis. Lancet 402, 571–584. https://doi.org/10.1016/S0140-6736(23)00966-2.

Lindemans, C.A., Calafiore, M., Mertelsmann, A.M., O'Connor, M.H., Dudakov, J.A., Jenq, R.R., Velardi, E., Young, L.F., Smith, O.M., Lawrence, G., et al. (2015). Interleukin-22 promotes intestinal-stem-cell-mediated epithelial regeneration. Nature *528*, 560–564. https://doi.org/10.1038/nature16460.

Meyer, A.R., Brown, M.E., McGrath, P.S., and Dempsey, P.J. (2022). Injury-induced cellular plasticity drives intestinal regeneration. Cell. Mol. Gastroenterol. Hepatol. *13*, 843–856. https://doi.org/10.1016/j.jcmgh.2021.12.005.

Nusse, Y.M., Savage, A.K., Marangoni, P., Rosendahl-Huber, A.K.M., Landman, T.A., de Sauvage, F.J., Locksley, R.M., and Klein, O.D. (2018). Parasitic helminths induce fetal-like reversion in the intestinal stem cell niche. Nature *559*, 109–113. https://doi.org/10.1038/s41586-018-0257-1.

Oshima, H., Kok, S.Y., Nakayama, M., Murakami, K., Voon, D.C.C., Kimura, T., and Oshima, M. (2019). Stat3 is indispensable for damage-induced crypt regeneration but not for Wnt-driven intestinal tumorigenesis. Faseb. J. *33*, 1873–1886. https://doi.org/10.1096/fj.201801176R.

Parikh, K., Antanaviciute, A., Fawkner-Corbett, D., Jagielowicz, M., Aulicino, A., Lagerholm, C., Davis, S., Kinchen, J., Chen, H.H., Alham, N.K., et al. (2019). Colonic epithelial cell diversity in health and inflammatory bowel disease. Nature *567*, 49–55. https://doi.org/10.1038/s41586-019-0992-y.

Philips, R.L., Wang, Y., Cheon, H., Kanno, Y., Gadina, M., Sartorelli, V., Horvath, C.M., Darnell, J.E., Jr., Stark, G.R., and O'Shea, J.J. (2022). The JAK-STAT pathway at 30: Much learned, much more to do. Cell *185*, 3857–3876. https://doi.org/10.1016/j.cell.2022.09.023.

Pickert, G., Neufert, C., Leppkes, M., Zheng, Y., Wittkopf, N., Warntjen, M., Lehr, H.A., Hirth, S., Weigmann, B., Wirtz, S., et al. (2009). STAT3 links IL-22 signaling in intestinal epithelial cells to mucosal wound healing. J. Exp. Med. *206*, 1465–1472. https://doi.org/10.1084/jem.20082683.

Pikkupeura, L.M., Bressan, R.B., Guiu, J., Chen, Y., Maimets, M., Mayer, D., Schweiger, P.J., Hansen, S.L., Maciag, G.J., Larsen, H.L., et al. (2023). Transcriptional and epigenomic profiling identifies YAP signaling as a key regulator of intestinal epithelium maturation. Sci. Adv. *9*, eadf9460. https://doi.org/10.1126/sciadv.adf9460.

Rao, D., Macias, E., Carbajal, S., Kiguchi, K., and DiGiovanni, J. (2015). Constitutive Stat3 activation alters behavior of hair follicle stem and progenitor cell populations. Mol. Carcinog. *54*, 121–133. https://doi.org/10.1002/mc.22080.

Serra, D., Mayr, U., Boni, A., Lukonin, I., Rempfler, M., Challet Meylan, L., Stadler, M.B., Strnad, P., Papasaikas, P., Vischi, D., et al. (2019). Self-organization and symmetry breaking in intestinal



organoid development. Nature 569, 66-72. https://doi.org/10. 1038/s41586-019-1146-y.

Shimokawa, M., Ohta, Y., Nishikori, S., Matano, M., Takano, A., Fujii, M., Date, S., Sugimoto, S., Kanai, T., and Sato, T. (2017). Visualization and targeting of LGR5(+) human colon cancer stem cells. Nature 545, 187-192. https://doi.org/10.1038/nature22081.

Smillie, C.S., Biton, M., Ordovas-Montanes, J., Sullivan, K.M., Burgin, G., Graham, D.B., Herbst, R.H., Rogel, N., Slyper, M., Waldman, J., et al. (2019). Intra- and inter-cellular rewiring of the human colon during ulcerative colitis. Cell 178, 714–730.e22. https://doi.org/10.1016/j.cell.2019.06.029.

Taniguchi, K., Wu, L.W., Grivennikov, S.I., de Jong, P.R., Lian, I., Yu, F.X., Wang, K., Ho, S.B., Boland, B.S., Chang, J.T., et al. (2015). A gp130-Src-YAP module links inflammation to epithelial regeneration. Nature 519, 57-62. https://doi.org/10.1038/ nature14228.

Tetteh, P.W., Basak, O., Farin, H.F., Wiebrands, K., Kretzschmar, K., Begthel, H., van den Born, M., Korving, J., de Sauvage, F., van Es, J.H., et al. (2016). Replacement of lost LGR5-positive stem cells through plasticity of their enterocyte-lineage daughters. Cell Stem Cell 18, 203-213. https://doi.org/10.1016/j.stem.2016. 01.001.

van Es, J.H., Sato, T., van de Wetering, M., Lyubimova, A., Yee Nee, A.N., Gregorieff, A., Sasaki, N., Zeinstra, L., van den Born, M., Korving, J., et al. (2012). Dll1+ secretory progenitor cells revert to stem cells upon crypt damage. Nat. Cell Biol. 14, 1099-1104. https:// doi.org/10.1038/ncb2581.

Yui, S., Azzolin, L., Maimets, M., Pedersen, M.T., Fordham, R.P., Hansen, S.L., Larsen, H.L., Guiu, J., Alves, M.R.P., Rundsten, C.F., et al. (2018). YAP/TAZ-dependent reprogramming of colonic epithelium links ECM remodeling to tissue regeneration. Cell Stem Cell 22, 35–49.e7. https://doi.org/10.1016/j.stem.2017. 11.001.